

# On-the-fly *ab initio* semiclassical evaluation of electronic coherences in polyatomic molecules reveals a simple mechanism of decoherence

Nikolay V. Golubev,<sup>\*</sup> Tomislav Begušić, and Jiří Vaníček<sup>†</sup>

Laboratory of Theoretical Physical Chemistry, Institut des Sciences et Ingénierie Chimiques,  
Ecole Polytechnique Fédérale de Lausanne (EPFL), CH-1015 Lausanne, Switzerland

(Dated: May 26, 2020)

Irradiation of a molecular system by an intense laser field can trigger dynamics of both electronic and nuclear subsystems. The lighter electrons usually move on much faster, attosecond time scale but the slow nuclear rearrangement damps ultrafast electronic oscillations, leading to the decoherence of the electronic dynamics within a few femtoseconds. We show that a simple, single-trajectory semiclassical scheme can evaluate the electronic coherence time in polyatomic molecules accurately by demonstrating an excellent agreement with full-dimensional quantum calculations. In contrast to numerical quantum methods, the semiclassical one reveals the physical mechanism of decoherence beyond the general blame on nuclear motion. In the propiolic acid, the rate of decoherence and the large deviation from the static frequency of electronic oscillations are quantitatively described with just two semiclassical parameters—the phase space distance and signed area between the trajectories moving on two electronic surfaces. Because it evaluates the electronic structure on the fly, the semiclassical technique avoids the “curse of dimensionality” and should be useful for preselecting molecules for experimental studies.

Recent progress in laser technologies [1–3] has revolutionized the field of atomic and molecular physics. In particular, tremendous developments of coherent light sources enabled the creation of sub-femtosecond laser pulses with remarkably well controlled parameters [4]. Using state-of-the-art lasers, one is able to initiate and probe processes that are driven solely by the electron correlation, i.e., to study and manipulate electron dynamics on its natural time scale [5].

Experimental measurements of the electron motion in isolated atoms were reported [6, 7], whereas a direct evidence of ultrafast electron dynamics in molecules remains a point of debate [8]. In particular, there are contradictions between recent experimental studies [9, 10] claiming to have observed the ultrafast electronic processes in molecules and theoretical investigations [11, 12] performed on systems of similar complexity. The disagreement is centered around the question on how strong is the influence of the slow nuclear motion on the dynamics of electronic density. Extensive *ab initio* calculations for several molecules [11, 12] demonstrated that the nuclear dynamics leads to the decoherence of the electronic wave packet on the time scale of a few femtoseconds which can make experimental observations of the electronic motion impossible. At the same time, long-lasting electronic coherences were reported for the ionized propiolic acid [13] and iodoacetylene [14], suggesting that the influence of nuclear motion on the electronic dynamics is very case-specific and requires careful investigation.

Understanding the interplay between the nuclear rearrangement and ultrafast electronic motion requires a concerted description of the electron-nuclear dynamics. Being one of the most powerful approaches for this purpose, the multi-configurational time-dependent Hartree (MCTDH) method [15–17] was recently applied for de-

scribing electronic coherence [11, 13]. Although this rigorous technique takes into account all quantum effects, such as tunneling and non-adiabatic transitions, it suffers from exponential scaling and also requires constructing global potential energy surfaces (PESs).

An alternative strategy for simulating coupled electron-nuclear dynamics employs a trajectory-guided Gaussian basis to represent the evolving wavepacket and an “on-the-fly” evaluation of the electronic structure. These “direct dynamics” approaches calculate the PESs along trajectories only, thus avoiding the precomputation of globally fitted surfaces, and sample only the relevant regions of the configuration space. Among these methods, the closest in spirit to MCTDH are the variational multi-configurational Gaussians (vMCG) [18–21], but many others exist, ranging from *ab initio* multiple spawning [22] and other Gaussian basis methods [23, 24] to more approximate mixed quantum-classical [25, 26] and semiclassical [27–29] approaches.

Treating electronic coherence with trajectory-based techniques was pioneered by Bearpark, Robb and co-workers [30–33] who propagated multiple trajectories representing an initially delocalized wave packet using Ehrenfest approximation. Although this technique captures decoherence due to a superposition of coherent oscillations with different frequencies appearing at the respective nuclear geometries, it completely ignores the decoherence due to the quantum motion of the wave packet resulting in the accumulation of phase along the propagated trajectory. The latter mechanism is referred to as the phase jitter [34] in general literature on quantum decoherence or, more specifically, as dephasing in the case of electron-nuclear processes. Allowing the wave packet to evolve quantum mechanically, dephasing mechanism was taken into account and the electronic coherence upon

ionization of a system was simulated in several molecules using the direct dynamics version of vMCG scheme [12] and its Ehrenfest-based variant [35].

Here, we use the thawed Gaussian approximation (TGA) [36–38], one of the simplest semiclassical approaches for molecular dynamics, to evaluate the influence of nuclear motion on the ultrafast electronic dynamics and to find a simple, yet detailed mechanism of decoherence, which is not available in basis set methods such as MCTDH or vMCG. Within the TGA, the nuclear wavefunction is described by a single Gaussian wave packet whose center follows Hamilton’s equations of motion and whose time-dependent width and phase are propagated using the local harmonic approximation of the PES.

We simulate coupled electron-nuclear dynamics taking place after outer-valence ionization of two polyatomic molecules: propiolic acid ( $\text{HC}_2\text{COOH}$ ) and its amide derivative propiolamide ( $\text{HC}_2\text{CONH}_2$ ). Propiolic acid provides us a perfect system for validating the semiclassical TGA because the electronic coherences in this molecule were recently calculated using a full quantum MCTDH approach [13]. The propiolamide molecule, in turn, is studied here for the first time.

The starting point of our investigations is a neutral molecule in its ground electronic and vibrational states. The ionization of the system performed by the ultrashort laser pulse can bring the molecule to a non-stationary superposition of ionic states, thus launching a coupled dynamics of electronic and nuclear wave packets. A coherent superposition of multiple electronic states triggers oscillations of the charge along a molecular chain. This purely electronic mechanism was termed *charge migration* [39, 40] to distinguish it from a more common charge transfer driven by nuclei [41]. Although the charge migration is governed by the electronic motion, it is strongly coupled with the nuclear dynamics and therefore can crucially affect the behavior of the whole molecule.

Previous calculations of the ionization spectrum of propiolic acid showed [13, 42] that, due to the electron correlation, the ground and the second excited ionic states of the molecule are a strong mixture of two one-hole configurations: an electron missing in the highest occupied molecular orbital (HOMO) and an electron missing in the HOMO–2. Therefore, a sudden removal of an electron either from HOMO or from HOMO–2 will create an electronic wave packet, which will initiate charge migration oscillations between the carbon triple bond and the carbonyl oxygen with a period of about 6.2 fs, determined by the energy gap between the first and the third cationic states [42]. Due to the planar geometry of the propiolic acid and a large energy gap between remaining ionic states, the indicated superposition can be obtained in an experiment by an appropriate orientation of the molecule with respect to the laser polarization.

To describe the ionization process, we used the

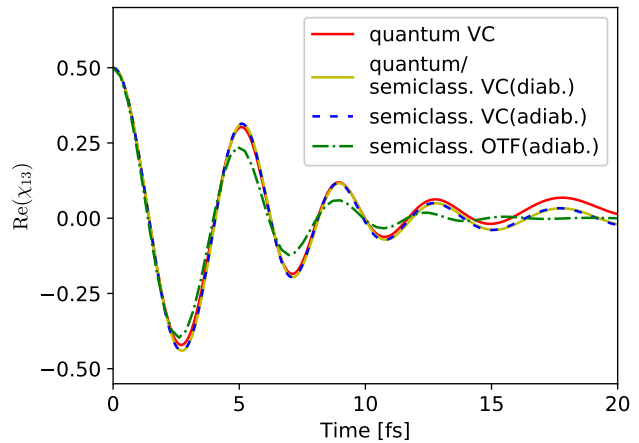


FIG. 1. Electronic coherence measured by the time-dependent overlap  $\chi_{13}(t)$  of the nuclear wave packets propagated on the first and third cationic states of propiolic acid after removal of a HOMO electron. Dynamics was performed with the full quantum MCTDH method (“quantum”) or with the semiclassical vertical-Hessian thawed Gaussian approximation (“semi-class.”), and either with the vibronic coupling (“VC”) or on-the-fly (“OTF”) Hamiltonian, both obtained at the *ab initio* many-body Green’s function ADC(3) level of theory. All simulations except the “quantum VC” calculation employed the diabatic approximation (“diab.”), which neglects nonadiabatic couplings between the diabatic states, or the adiabatic approximation (“adiab.”), which neglects nonadiabatic couplings between adiabatic states.

non-Dyson algebraic-diagrammatic-construction (ADC) scheme [43] to represent the one-particle Green’s function. We chose a rather computationally expensive ADC method because it allows treating the ionization process explicitly starting from the neutral state of a system. This important advantage over other, more conventional electronic structure approaches allows us to estimate populations of the resulting ionic states created after removal of an electron from a molecule. [See Sec. I Supplementary Material (SM) for details.]

Within the sudden and Franck–Condon approximations, the ionization is modelled by projecting the ground (electronic and nuclear) neutral state of a molecule onto the ionic subspace of the system. After ionization, a single nuclear Gaussian wave packet on each involved ionic surface is propagated independently from the others (non-adiabatic effects are neglected). The center of each Gaussian is guided by a single classical trajectory, while the width and phase are propagated using the single-Hessian [44] variant of the TGA.

Within the Born–Huang representation [45] of the molecular wavefunction, the expectation value of an electronic operator  $\hat{O}(\mathbf{r}, \mathbf{R})$  can be expressed as

$$\langle \hat{O} \rangle(t) = \sum_{i,j} \int \chi_i^*(\mathbf{R}, t) O_{ij}(\mathbf{R}) \chi_j(\mathbf{R}, t) d\mathbf{R}, \quad (1)$$

where  $O_{ij}(\mathbf{R}) = \int \Phi_i^*(\mathbf{r}, \mathbf{R}) \hat{O}(\mathbf{r}, \mathbf{R}) \Phi_j(\mathbf{r}, \mathbf{R}) d\mathbf{r}$  denote the  $\mathbf{R}$ -dependent matrix elements of the electronic operator between electronic states  $i$  and  $j$ , and the quantities  $\chi_i(\mathbf{R}, t)$  are the time-dependent nuclear wave packets propagated on the corresponding PESs.

If both the operator  $\hat{O}(\mathbf{r}, \mathbf{R})$  and the electronic states  $\{\Phi_i(\mathbf{r}, \mathbf{R})\}$  depend weakly on nuclear coordinates  $\mathbf{R}$ , Eq. (1) can be further simplified as

$$\langle \hat{O} \rangle(t) \approx \sum_{i,j} O_{ij} \chi_{ij}(t), \quad (2)$$

where the nuclear overlaps  $\chi_{ij}(t) = \int \chi_i^*(\mathbf{R}, t) \chi_j(\mathbf{R}, t) d\mathbf{R}$  represent the populations of electronic states when  $i = j$  and the electronic coherences [11–13] when  $i \neq j$ . Equation (2) shows that the factors  $\chi_{ij}(t)$  provide the only source of time dependence in the expectation value of the electronic operator and thus can serve as convenient properties to quantify the decoherence time. Electronic coherence evaluated as the nuclear overlap  $\chi_{ij}(t)$  is a special case of *fidelity amplitude* (also called Loschmidt echo), a quantity measuring sensitivity of quantum dynamics to perturbations and defined as the overlap at time  $t$  of two wavepackets, initially the same but propagated with different Hamiltonians [46–53].

We computed the electronic coherences  $\chi_{ij}(t)$  generated after ionizing an electron from the HOMO of the propiolic acid; the initial molecular wave packet was an equally weighted and phase-synchronized superposition of the first and third cationic states. Figure 1 shows the electronic coherence evaluated by five different schemes. We adopted the vibronic-coupling (VC) Hamiltonian from Ref. [13] to perform MCTDH simulations taking into account all nuclear degrees of freedom. The full quantum-mechanical calculations show (red solid line in Fig. 1) that the electronic oscillations are strongly influenced by nuclear motion—the coherences are completely suppressed within first 15 fs [13].

To validate the applicability of the TGA, we performed semiclassical calculations using *adiabatic* version of the VC Hamiltonian, where the PESs were obtained by diagonalizing the four-state VC model used in the MCTDH calculations. Our simulation shows (blue dashed line in Fig. 1) that on the short time scale the TGA gives results almost identical to the full quantum MCTDH calculations. The small deviations start to appear at longer times due to the nonadiabatic effects, neglected in the TGA. Note that TGA is exact within the VC model when the diabatic PESs are not coupled to each other, and therefore provides results identical to the MCTDH simulations performed on such VC Hamiltonian (yellow solid line in Fig. 1).

We also performed semiclassical calculations with on-the-fly evaluation of the electronic structure at the same *ab initio* level of theory as that used in the construction of the VC Hamiltonian (green dash-dotted line in Fig. 1).

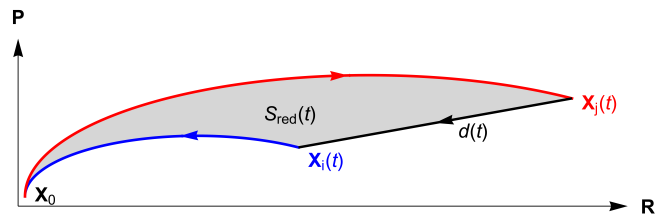


FIG. 2. Geometric interpretation of Eq. (5): The reduced action  $S_{\text{red}}$  is the gray phase-space area enclosed by the curve  $\mathbf{C}$  consisting of the classical trajectory propagated in state  $i$  with potential energy  $V_i$  and connecting  $\mathbf{X}_i(t)$  with  $\mathbf{X}_0$  (blue curve), classical trajectory propagated in state  $j$  with potential energy  $V_j$  and connecting  $\mathbf{X}_0$  with  $\mathbf{X}_j(t)$  (red curve), and a straight (black) line connecting  $\mathbf{X}_j(t)$  with  $\mathbf{X}_i(t)$ . The correct sign of  $S_{\text{red}}$  is obtained by taking the curve integral along  $\mathbf{C}$  in the direction indicated by the arrows. The phase space distance between the final points  $\mathbf{X}_j(t)$  and  $\mathbf{X}_i(t)$ , given by the length  $d$  of the black line segment, determines the coherence decay [i.e., the decay of  $|\chi_{ij}(t)|$ ], while the reduced action  $S_{\text{red}}$ , equal to the gray area, affects the frequency of oscillations of the coherence  $\chi_{ij}(t)$ .

In this case, the wave packet can potentially evolve beyond a simple model used for fitting PESs. In particular, VC Hamiltonian typically uses a rather primitive approximation of PESs for nuclear configurations formed by superposition of normal modes. Allowing the wave packet to evolve according to the exact Hamiltonian computed on the fly makes it possible to visit nuclear regions inaccessible within the VC Hamiltonian and thus to take anharmonicity effects into account (see Sec. II of SM for details). This is reflected in our on-the-fly calculations, which predict the electronic motion with a similar oscillation period, but a slightly faster decay of the electronic coherence than within the VC model. Remarkably, because the effect of using the on-the-fly potential is much larger than the effect of including the nonadiabatic couplings, the semiclassical on-the-fly result of the TGA is most likely more accurate than the quantum result of the MCTDH calculation with the VC model!

In Sec. III of SM, we derive an analytical expression

$$\chi_{ij}(t) = e^{-d(t)^2/4\hbar} e^{iS(t)/\hbar} \quad (3)$$

for the semiclassically evaluated coherence in case the two Gaussians have fixed widths. Here  $d(t)$  is phase-space distance (in mass- and frequency-scaled phase-space coordinates  $\mathbf{R}$  and  $\mathbf{P}$ ) between the centers of the two Gaussian wavepackets at time  $t$ ,

$$S(t) = S_{\text{red}}(t) - \Delta E t, \quad (4)$$

is the classical action,  $\Delta E = V_j(\mathbf{R}_0) - V_i(\mathbf{R}_0)$  is the energy gap at the initial point  $\mathbf{R}_0$ , and

$$S_{\text{red}}(t) = \oint_{\mathbf{C}} \mathbf{P}^T \cdot d\mathbf{R} \quad (5)$$

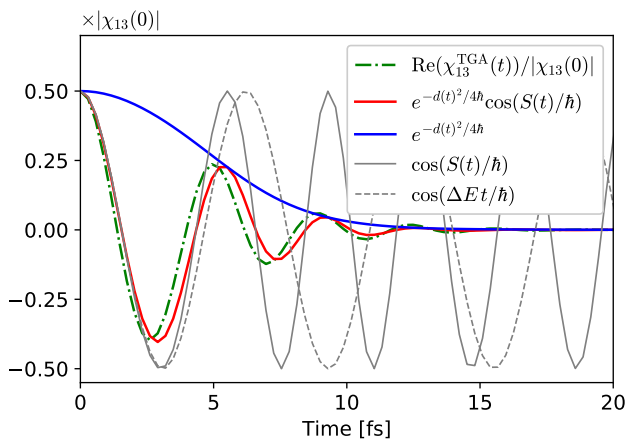


FIG. 3. Semiclassical analysis of the electronic coherence  $\chi_{13}(t)$  from Fig. 1. Comparison of the coherence computed with the on-the-fly version of TGA (green dash-dotted line), analytical semiclassical expression (3) (red solid line), factors describing the decay (blue solid line) and oscillations (gray solid line) of coherence in the presence of nuclear motion, and the undamped coherence in the absence of nuclear motion (gray dashed line).

is the reduced action equal to the signed area within the closed curve  $\mathbf{C}$  shown in Fig. 2 [52].

The analytical expression (3) provides a simple, semiclassical interpretation of the effect of nuclear dynamics on electronic coherence (see Fig. 3): The diverging nuclear trajectories affect not only the absolute value of  $\chi_{ij}(t)$ , which, as expected, decays as a Gaussian function of the phase-space distance  $d(t)$ , but also frequency of electronic oscillations. In the absence of nuclear motion, the electronic coherence would oscillate with frequency  $\Delta E/\hbar$ , but now, due to nuclear dynamics, the phase of electronic oscillations at time  $t$  is modified by the area  $S_{\text{red}}(t)$  divided by  $\hbar$  [see Eqs. (3), (4), and (5)]. It is easy to see that if the potential energy surfaces are simply vertically shifted, i.e., if  $V_j = V_i + \Delta E$ , then  $\mathbf{X}_i = \mathbf{X}_j$  and  $d = S_{\text{red}} = 0$ , implying that the electronic coherence  $\chi_{ij}(t)$  is not affected by nuclear dynamics.

Let us turn to the electron-nuclear dynamics driven by the ionization of the propiolamide. Similar to the spectrum of the propiolic acid [42], in the energy range 10–14 eV only the four states shown in Fig. 2 in Sec. IV of the SM are present. The strong electron correlation between valence orbitals in the neutral propiolamide leads to appearance of the almost equal in weights one-hole configurations in the ionic states. Therefore, an ultra-short (sudden) ionization of the molecule will inevitably create an electronic wave packet and trigger dynamics of the electron density between the carbon triple bond and amide moiety. The molecule is planar and thus belongs to the  $C_s$  symmetry group which allows assignment of the ionic states to two irreducible representations: the second and fourth states belong to the  $A'$ , while the first

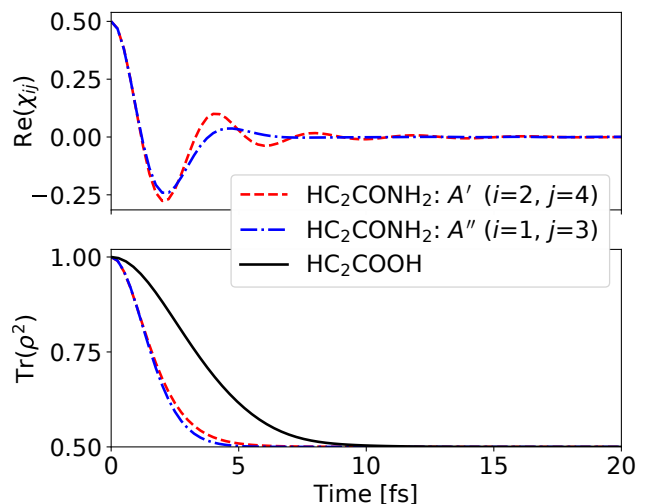


FIG. 4. Top panel: Time evolution of the electronic coherences  $\chi_{ij}(t)$  created by the equally weighted coherent superposition of the second and fourth cationic states (ionization from the HOMO-1,  $A'$  symmetry), and the first and third cationic states (ionization from the HOMO,  $A''$  symmetry). Bottom panel: Comparison of the electronic purity function  $\text{Tr}(\rho^2)$  for the propiolamide and propiolic acid molecules.

and third states to  $A''$ . As for propiolic acid, orientation of the propiolamide with respect to polarization of the ionizing laser field can be used to populate only the states of interest.

Figure 4 shows the evolution of the electronic coherence in the propiolamide. Taking advantage of the molecular symmetry, we simulate dynamics occurring after removal of the HOMO (populating the first and third cationic states) and HOMO-1 (populating the second and fourth cationic states) electrons. Starting from the equally weighted and phase-matched superposition of the electronic states, in both cases the nuclear motion perturbs electronic oscillations and leads to decoherence. Coherence times of different molecules can be compared using the purity  $\text{Tr}(\rho(t)^2)$  [11], where the electronic density matrix  $\rho(t)$  is related to the matrix of nuclear overlaps from Eq. (2) by transposition:  $\rho_{ij}(t) = \chi_{ji}(t)$ . Due to decoherence, the purity decays from the value  $\text{Tr}(\rho(0)^2) = 1$  for the initially pure state to the value  $1/n$  for the equally weighted mixture of  $n$  states.

Our simulations demonstrate that, contrary to the propiolic acid molecule, for which long-lasting coherences were observed (see bottom panel of Fig. 4 and also Ref. [13]), the initially pure superpositions in the propiolamide evolve to mixed states in just a few femtoseconds. Importantly, the energy gaps between the involved electronic states of propiolamide are larger than those for the propiolic acid (see Fig. 2 of SM and Ref. [42]), which leads to faster oscillations of electronic density along the molecular chain. Despite the rather short co-

herence time, due to the faster charge migration the electronic density in the propiolamide has enough time to perform one clear oscillation (see Fig. 4 above and Fig. 3 of SM). Moreover, the existence of the strong hole-mixing in both symmetries of the propiolamide can be used to induce oscillations of the charge along different directions in the molecule. Dependence of the charge migration on the molecular orientation provides an important advantage for experimental measurements utilizing the time-resolved high-harmonic generation (HHG) spectroscopy employed recently by Wörner and co-workers [5]. Alignment of the molecule with respect to the pump pulse should be reflected in the resulting HHG spectra and thus can be used as a direct evidence of the ultrafast electron dynamics.

Although trajectory-based direct dynamics methods were previously used to estimate electronic coherences in various polyatomic molecules [12, 35], converged results typically required a large number of trajectories. The vMCG used in these studies take into account non-adiabatic transitions and tunneling effects, but require solving rather complicated equations of motion and make interpreting obtained results less intuitive than the simple picture provided here in Eq. (3) and Figs. 2 and 3. Our approach based on the TGA can be viewed as a very special case of far more general vMCG—namely, it can be classified as a single-Gaussian, non-variational, multi-set, non-frozen, adiabatic, single-Hessian version of vMCG. In contrast to the application of vMCG in Refs. [12, 35], our implementation of the TGA uses a multi-set approach, where a *single* Gaussian function with *relaxed* parameters is used for every involved electronic state. By approximately taking into account quantum properties of the wave packet, such as its width and phase, the TGA captures the dephasing mechanism while maintaining sufficient accuracy, especially at short time scales. A detailed comparison of the TGA and vMCG is provided in Sec. V of SM—remarkably, the TGA, which uses only a single classical trajectory per electronic state, yields in the propiolic acid better results than the single-set version of vMCG with 31 variational trajectories (see Fig. 4 in SM). While the multi-set version of vMCG gives similar results to TGA also with 1 Gaussian, no improvement is seen by using 8 Gaussians (Fig. 4 of SM). In the TGA, using only two classical trajectories was not only sufficient but also crucial for revealing the simple physical mechanism of decoherence.

The semiclassical vertical-Hessians TGA used in this paper can be further improved by calculating Hessians along the propagated trajectory and thus taking into account more complicated situations, e.g., dissociation of a molecule. Extensions of the TGA, such as the extended thawed Gaussian approximation [54, 55] or Hagedorn wavepackets [38, 56], which propagate a Gaussian multiplied by a linear or general polynomial, can make on-the-fly semiclassical simulations even more accurate.

In conclusion, we implemented a simple and efficient on-the-fly semiclassical approach to understand the effects of nuclear motion on electronic coherence in molecules. Although the propiolic acid and propiolamide have very similar ionization spectra, our calculations predict that their electronic coherence times differ substantially. The simple method was validated by comparison with the full-dimensional quantum calculations performed using the MCTDH and vMCG methods. As suggested by Fig. 1, neglecting the nonadiabatic couplings by the TGA may not be a severe approximation because, even in systems with strong couplings, the nonadiabatic effects typically start playing a significant role only at times longer than the ultrashort decoherence time scale. If one suspects an exceptional importance of nonadiabatic effects even at times before the electronic coherence has decayed to zero, it is possible to validate the applicability of the TGA without performing expensive quantum simulations by verifying adiabaticity with on-the-fly semiclassical calculations based, e.g., on surface hopping [25] or multiple-surface dephasing representation [57–60].

Despite its limitations, the presented technique for evaluating coherence can help breaking the “curse of dimensionality” appearing in the quantum treatment of large molecules, which can be crucial for full-dimensional simulations of ultrafast electronic processes in biologically relevant systems [61]. Being able to treat molecules with a few hundred atoms, this technique can help shed light on the continuing debates on the role of quantum coherence in biology [62], quickly preselect molecules suitable for further experimental investigations, and support theoretically recent experimental observations of attosecond electron dynamics in realistic molecular systems.

Authors thank Alexander Kuleff for many valuable discussions and the Swiss National Science Foundation for financial support through the NCCR MUST (Molecular Ultrafast Science and Technology) Network. N. V. G. acknowledges the support by the Branco Weiss Fellowship—Society in Science, administered by the ETH Zürich.

---

\* nik.v.golubev@gmail.com

† jiri.vanicek@epfl.ch

- [1] F. Krausz and M. Ivanov, *Rev. Mod. Phys.* **81**, 163 (2009).
- [2] L. Young, K. Ueda, M. Gühr, P. H. Bucksbaum, M. Simon, S. Mukamel, N. Rohringer, K. C. Prince, C. Masciovecchio, M. Meyer, A. Rudenko, D. Rolles, C. Bostedt, M. Fuchs, D. A. Reis, R. Santra, H. Kapteyn, M. Murnane, H. Ibrahim, F. Légaré, M. Vrakking, M. Isinger, D. Kroon, M. Gisselbrecht, A. L’Huillier, H. J. Wörner, and S. R. Leone, *J. Phys. B: At., Mol. Opt. Phys.* **51**, 032003 (2018).
- [3] J. Mauritsson, G. Vampa, and C. Vozzi, *J. Opt.* **20**, 110201 (2018).

- [4] F. Krausz, Phys. Scr. **91**, 063011 (2016).
- [5] P. M. Kraus, B. Mignolet, D. Baykusheva, A. Rupenyan, L. Horny, E. F. Penka, G. Grassi, O. I. Tolstikhin, J. Schneider, F. Jensen, L. B. Madsen, A. D. Bandrauk, F. Remacle, and H. J. Wörner, Science **350**, 790 (2015).
- [6] E. Goulielmakis, Z.-H. Loh, A. Wirth, R. Santra, N. Rohringer, V. S. Yakovlev, S. Zherebtsov, T. Pfeifer, A. M. Azzeer, M. F. Kling, S. R. Leone, and F. Krausz, Nature **466**, 739 (2010).
- [7] X. Xie, S. Roither, D. Kartashov, E. Persson, D. G. Arbó, L. Zhang, S. Gräfe, M. S. Schöffler, J. Burgdörfer, A. Baltuška, and M. Kitzler, Phys. Rev. Lett. **108**, 193004 (2012).
- [8] F. Lépine, M. Y. Ivanov, and M. J. J. Vrakking, Nat. Photonics **8**, 195 (2014).
- [9] F. Calegari, D. Ayuso, A. Trabattoni, L. Belshaw, S. De Camillis, S. Anumula, F. Frassetto, L. Poletto, A. Palacios, P. Decleva, J. B. Greenwood, F. Martin, and M. Nisoli, Science **346**, 336 (2014).
- [10] M. Lara-Astiaso, M. Galli, A. Trabattoni, A. Palacios, D. Ayuso, F. Frassetto, L. Poletto, S. De Camillis, J. Greenwood, P. Decleva, I. Tavernelli, F. Calegari, M. Nisoli, and F. Martín, J. Phys. Chem. Lett. **9**, 4570 (2018).
- [11] C. Arnold, O. Vendrell, and R. Santra, Phys. Rev. A **95**, 033425 (2017).
- [12] M. Vacher, M. J. Bearpark, M. A. Robb, and J. a. P. Malhado, Phys. Rev. Lett. **118**, 083001 (2017).
- [13] V. Despré, N. V. Golubev, and A. I. Kuleff, Phys. Rev. Lett. **121**, 203002 (2018).
- [14] D. Jia, J. Manz, and Y. Yang, J. Phys. Chem. Lett. **10**, 4273 (2019).
- [15] H.-D. Meyer, U. Manthe, and L. S. Cederbaum, Chem. Phys. Lett. **165**, 73 (1990).
- [16] A. Raab, G. A. Worth, H.-D. Meyer, and L. S. Cederbaum, J. Chem. Phys. **110**, 936 (1999).
- [17] M. Beck, A. Jäckle, G. Worth, and H.-D. Meyer, Phys. Rep. **324**, 1 (2000).
- [18] I. Burghardt, H.-D. Meyer, and L. S. Cederbaum, J. Chem. Phys. **111**, 2927 (1999).
- [19] G. A. Worth and I. Burghardt, Chem. Phys. Lett. **368**, 502 (2003).
- [20] G. Worth, M. Robb, and B. Lasorne, Mol. Phys. **106**, 2077 (2008).
- [21] M. Šulc, H. Hernández, T. J. Martínez, and J. Vaníček, J. Chem. Phys. **139**, 034112 (2013).
- [22] B. F. E. Curchod and T. J. Martínez, Chem. Rev. **118**, 3305 (2018).
- [23] D. V. Shalashilin and M. S. Child, J. Chem. Phys. **121**, 3563 (2004).
- [24] K. Saita and D. V. Shalashilin, J. Chem. Phys. **137**, 22A506 (2012).
- [25] J. C. Tully, J. Chem. Phys. **93**, 1061 (1990).
- [26] X. Li, J. C. Tully, H. B. Schlegel, and M. J. Frisch, J. Chem. Phys. **123**, 084106 (2005).
- [27] M. F. Herman and E. Kluk, Chem. Phys. **91**, 27 (1984).
- [28] J. Tatchen and E. Pollak, J. Chem. Phys. **130**, 041103 (2009).
- [29] M. Ceotto, S. Atahan, G. F. Tantardini, and A. Aspuru-Guzik, J. Chem. Phys. **130**, 234113 (2009).
- [30] M. Vacher, D. Mendive-Tapia, M. J. Bearpark, and M. A. Robb, J. Chem. Phys. **142**, 094105 (2015).
- [31] M. Vacher, L. Steinberg, A. J. Jenkins, M. J. Bearpark, and M. A. Robb, Phys. Rev. A **92**, 040502 (2015).
- [32] A. J. Jenkins, M. Vacher, M. J. Bearpark, and M. A. Robb, J. Chem. Phys. **144**, 104110 (2016).
- [33] A. J. Jenkins, M. Vacher, R. M. Twidale, M. J. Bearpark, and M. A. Robb, J. Chem. Phys. **145**, 164103 (2016).
- [34] G. A. Fiete and E. J. Heller, Phys. Rev. A **68**, 022112 (2003).
- [35] A. J. Jenkins, K. E. Spinlove, M. Vacher, G. A. Worth, and M. A. Robb, J. Chem. Phys. **149**, 094108 (2018).
- [36] E. J. Heller, J. Chem. Phys. **62**, 1544 (1975).
- [37] T. Begušić, J. Roulet, and J. Vaníček, J. Chem. Phys. **149**, 244115 (2018).
- [38] C. Lasser and C. Lubich, (2020), arXiv:2002.00624 [math.NA].
- [39] L. Cederbaum and J. Zobeley, Chem. Phys. Lett. **307**, 205 (1999).
- [40] A. I. Kuleff and L. S. Cederbaum, J. Phys. B: At., Mol. Opt. Phys. **47**, 124002 (2014).
- [41] S. Sun, B. Mignolet, L. Fan, W. Li, R. D. Levine, and F. Remacle, J. Phys. Chem. A **121**, 1442 (2017).
- [42] N. V. Golubev, V. Despré, and A. I. Kuleff, J. Mod. Opt. **64**, 1031 (2017).
- [43] J. Schirmer, A. B. Trofimov, and G. Stelter, J. Chem. Phys. **109**, 4734 (1998).
- [44] T. Begušić, M. Cordova, and J. Vaníček, J. Chem. Phys. **150**, 154117 (2019).
- [45] M. Born and K. Huang, *Dynamical Theory of Crystal Lattices*, Oxford Classic Texts in the Physical Sciences (Oxford University Press, Oxford, 1954).
- [46] A. Peres, Phys. Rev. A **30**, 1610 (1984).
- [47] R. A. Jalabert and H. M. Pastawski, Phys. Rev. Lett. **86**, 2490 (2001).
- [48] J. Vaníček, Phys. Rev. E **73**, 046204 (2006).
- [49] T. Gorin, T. Prosen, T. H. Seligman, and M. Žnidarič, Phys. Rep. **435**, 33 (2006).
- [50] P. Jacquod and C. Petitjean, Adv. Phys. **58**, 67 (2009).
- [51] C. Mollica and J. Vaníček, Phys. Rev. Lett. **107**, 214101 (2011).
- [52] E. Zambrano and A. M. Ozorio de Almeida, Phys. Rev. E **84**, 045201(R) (2011).
- [53] A. Goussev, R. A. Jalabert, H. M. Pastawski, and D. Wisniacki, Scholarpedia **7**, 11687 (2012).
- [54] S.-Y. Lee and E. J. Heller, J. Chem. Phys. **76**, 3035 (1982).
- [55] A. Patoz, T. Begušić, and J. Vaníček, J. Phys. Chem. Lett. **9**, 2367 (2018).
- [56] G. A. Hagedorn, Ann. Phys. (N. Y.) **269**, 77 (1998).
- [57] T. Zimmermann and J. Vaníček, J. Chem. Phys. **132**, 241101 (2010).
- [58] T. Zimmermann and J. Vaníček, J. Chem. Phys. **136**, 094106 (2012).
- [59] T. Zimmermann and J. Vaníček, J. Chem. Phys. **137**, 22A516 (2012).
- [60] A. Prlj, T. Begušić, Z. T. Zhang, G. C. Fish, M. Wehrle, T. Zimmermann, S. Choi, J. Roulet, J.-E. Moser, and J. Vaníček, J. Chem. Theory Comput. **16**, 2617 (2020).
- [61] F. Calegari, A. Trabattoni, A. Palacios, D. Ayuso, M. C. Castrovilli, J. B. Greenwood, P. Decleva, F. Martín, and M. Nisoli, J. Phys. B: At., Mol. Opt. Phys. **49**, 142001 (2016).
- [62] N. Lambert, Y.-N. Chen, Y.-C. Cheng, C.-M. Li, G.-Y. Chen, and F. Nori, Nat. Phys. **9**, 10 (2013).



# Supplementary Material for “On-the-fly *ab initio* semiclassical evaluation of electronic coherences in polyatomic molecules reveals a simple mechanism of decoherence”

Nikolay V. Golubev,<sup>\*</sup> Tomislav Begušić, and Jiří Vaníček<sup>†</sup>

*Laboratory of Theoretical Physical Chemistry,*

*Institut des Sciences et Ingénierie Chimiques,*

*Ecole Polytechnique Fédérale de Lausanne (EPFL), CH-1015 Lausanne, Switzerland*

(Dated: May 26, 2020)

## Abstract

In the Letter, we have shown how the thawed Gaussian approximation (TGA) [1, 2] can be used to compute electronic coherence time in polyatomic molecules. Here, we present additional details of the calculations and results mentioned in the main text. After describing details of electronic structure computations in Sec. I, in Sec. II we discuss advantages of the on-the-fly approach over the previously reported fully quantum calculations of the electron-nuclear dynamics in the propiolic acid molecule [3] performed using the multi-configurational time-dependent Hartree (MCTDH) [4, 5] method on the vibronic coupling (VC) model. In Sec. III, we derive a simple semiclassical expression providing an intuitive phase-space interpretation of the decoherence presented in the main text. Section IV contains further details of the calculations of decoherence in the propiolamide. Finally, in Sec. V we include a detailed comparison of the TGA with the variational multi-configurational Gaussians (vMCG) method [6, 7], which was recently reviewed in Ref. [8] and applied to study electronic coherence in several molecules [9, 10].

---

<sup>\*</sup> nik.v.golubev@gmail.com

<sup>†</sup> jiri.vanicek@epfl.ch

## I. DETAILS OF ELECTRONIC STRUCTURE CALCULATIONS

Ionization potentials of propiolic acid and propiolamide molecules were calculated using the third-order ADC [ADC(3)] scheme [11] consistent with the exact Green’s function up to the third order of perturbation theory with respect to the Hartree–Fock reference Hamiltonian. Standard double-zeta plus polarization (DZP) basis sets [12] were employed to construct the noncorrelated reference states. Ground-state geometries of the neutral molecules were optimized using the density functional theory [13] with the B3LYP functional [14]. The optimization was done with Gaussian 16 package [15].

## II. COMPARISON OF TRAJECTORIES PROPAGATED USING THE VIBRONIC COUPLING AND ON-THE-FLY HAMILTONIANS

Whereas the direct dynamics version of the thawed Gaussian approximation (TGA) takes into account the anharmonicity at least partially, the VC Hamiltonian employs the harmonic approximation for fitting the potential energy surfaces (PESs). Clearly, this approximate treatment of the PESs can lead to substantial differences between “real” and approximate dynamics. Moreover, vibronic coupling (VC) Hamiltonian utilizes a rather primitive representation of PESs for nuclear configurations located “between” normal modes (i.e. such configurations which are formed by superposition of normal modes). The direct dynamics approach, in turn, operates with forces computed on the fly and thus makes it possible to visit nuclear regions that may be accidentally missed in the VC Hamiltonian. To investigate such effects, in Fig. 1 we show trajectories followed by the centers of Gaussian wave packets propagated on two surfaces associated with the two electronic states involved in the dynamics.

The top and bottom panels of the figure show evolution of classical trajectories along the fastest (high frequency) and slowest (low frequency) normal modes of the system, respectively. The fast mode has almost no effect on the overall decoherence because the trajectories propagated on the two involved surfaces are almost the same, regardless whether the calculation uses the VC or on-the-fly approach. Due to the anharmonicity of the two PESs, the on-the-fly classical trajectories gradually drift from the equilibrium point, but this drift is almost the same for the trajectories on the two surfaces and, as a result, has almost no



effect on the overall decoherence. The situation is different for the slow mode (see bottom panel of Fig. 1), where trajectories on the two surfaces move in opposite directions, resulting in fast decoherence of nuclear wave packets propagating in the two states. Because the two on-the-fly trajectories diverge faster than the corresponding VC trajectories, the decay of electronic coherence is faster in the case of on-the-fly propagation than for the precomputed VC Hamiltonian. Similar analysis can be repeated for all modes and explains the slightly faster decay of overall coherence in the on-the-fly calculation observed in Fig. 1 of the main text. Note that such a simple and intuitive description of decoherence is available only in the multi-set approach and, as we show below, is further simplified in the TGA setting, with a single Gaussian on each surface.

### III. PHASE-SPACE DESCRIPTION OF DECOHERENCE

We now derive an analytical semiclassical expression for the time-dependent coherence, which yields a simple phase-space interpretation of the effect of nuclear dynamics on the decay rate and frequency of electronic coherence oscillations. The derivation and interpretation is simplified by further assuming the width of the Gaussian wavepackets to be fixed.

Let us consider electronic coherence evaluated as the overlap

$$\chi_{12}(t) = \int d\mathbf{R} \chi_1^*(\mathbf{R}, t) \chi_2(\mathbf{R}, t) \quad (1)$$

of two frozen nuclear Gaussian wavepackets

$$\chi_i(\mathbf{R}, t) = \det \left( \frac{\mathbf{m} \cdot \boldsymbol{\Omega}}{\pi \hbar} \right)^{1/4} e^{-\frac{1}{2\hbar} [\mathbf{R} - \mathbf{R}_i(t)]^T \cdot \mathbf{m}^{1/2} \cdot \boldsymbol{\Omega} \cdot \mathbf{m}^{1/2} \cdot [\mathbf{R} - \mathbf{R}_i(t)] + \frac{i}{\hbar} \mathbf{P}_i(t)^T \cdot [\mathbf{R} - \mathbf{R}_i(t)] + \frac{i}{\hbar} \gamma_i(t)}, \quad i \in \{1, 2\}, \quad (2)$$

evolved with two different Hamiltonians  $H_1$  and  $H_2$  from the same initial Gaussian centered at  $\mathbf{R}_0$  and  $\mathbf{P}_0 = \mathbf{0}$ . Here  $\boldsymbol{\Omega}$  is the matrix of vibrational frequencies in the electronic ground state, the fixed width matrix is given by  $\mathbf{m}^{1/2} \cdot \boldsymbol{\Omega} \cdot \mathbf{m}^{1/2}$  because the initial state was a vibrational ground state of the ground electronic state, the pair  $(\mathbf{R}_i, \mathbf{P}_i) \equiv \mathbf{X}_i$  denotes the phase-space center of the Gaussian,  $\gamma_i = S_i - [\hbar \text{Tr}(\boldsymbol{\Omega})/2]t$  is the time-dependent phase of the wavepacket, and  $S_i$  is the classical action along the classical path connecting  $\mathbf{X}_0$  and  $\mathbf{X}_i$ . Before computing the overlap  $\chi_{12}(t)$  explicitly, we introduce mass- and frequency-scaled

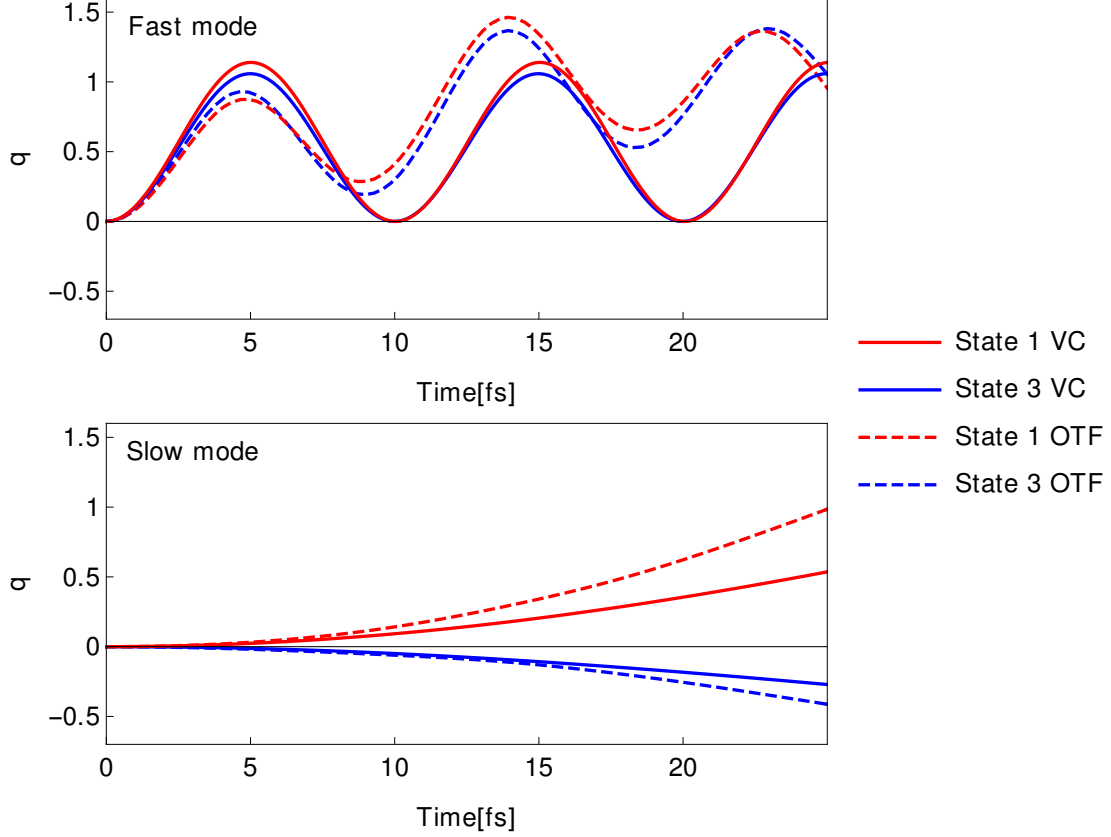


FIG. 1: Classical trajectories followed by the centers of Gaussian wave packets propagated on the fly (OTF, dashed lines) or using the vibronic coupling Hamiltonian (VC, solid lines) on the potential energy surface associated with the first (red color) or third (blue color) cationic state. Normal mode coordinates of these trajectories are shown only for the fastest (top panel) and slowest (bottom panel) modes of the propiolic acid molecule. The fast mode, despite its richer dynamics, has a very limited effect on the decay of the coherence because the nuclear wave packets exhibit almost identical dynamics in both states. In contrast, the wave packets propagated in the two states move to opposite directions along the slow mode which leads to decoherence.

coordinates and momenta

$$\mathbf{R}' := \Omega^{1/2} \cdot \mathbf{m}^{1/2} \cdot \mathbf{R}, \quad (3)$$

$$\mathbf{P}' := \Omega^{-1/2} \cdot \mathbf{m}^{-1/2} \cdot \mathbf{P}, \quad (4)$$

(and immediately drop the prime superscripts for simplicity) to write the wavepacket as

$$\chi_i(\mathbf{R}, t) = \exp \left\{ -\frac{1}{2\hbar} [\mathbf{R} - \mathbf{R}_i(t)]^2 + \frac{i}{\hbar} \mathbf{P}_i(t)^T \cdot [\mathbf{R} - \mathbf{R}_i(t)] + \frac{i}{\hbar} \gamma_i(t) \right\}. \quad (5)$$

The overlap is then given analytically as

$$\chi_{12}(t) = e^{-d(t)^2/4\hbar} e^{iS(t)/\hbar}, \quad (6)$$

where

$$d(t) = |\mathbf{X}_2(t) - \mathbf{X}_1(t)| = \sqrt{|\mathbf{R}_2(t) - \mathbf{R}_1(t)|^2 + |\mathbf{P}_2(t) - \mathbf{P}_1(t)|^2} \quad (7)$$

is the phase-space distance between the centers of the two Gaussian wavepackets and

$$S(t) = \frac{1}{\hbar} \left[ (S_2 - S_1) - \bar{\mathbf{P}}^T \cdot \Delta \mathbf{R} \right], \quad (8)$$

$$\bar{\mathbf{P}} = \frac{1}{2} (\mathbf{P}_1(t) + \mathbf{P}_2(t)), \quad (9)$$

$$\Delta \mathbf{R} = \mathbf{R}_2(t) - \mathbf{R}_1(t). \quad (10)$$

We now rewrite the action  $S_i$  on each surface as

$$S_i(t) = \int_0^t L_i d\tau \quad (11)$$

$$= \int_0^t (\mathbf{P}_i^T \cdot \dot{\mathbf{R}} - H_i) d\tau \quad (12)$$

$$= \int_{\mathbf{R}_0}^{\mathbf{R}_i(t)} \mathbf{P}_i^T \cdot d\mathbf{R} - tV_i(\mathbf{R}_0). \quad (13)$$

$L_i$  is the Lagrangian evaluated along the classical path  $\mathbf{X}_i$ ,  $H_i(\mathbf{X}_i) = H_i(\mathbf{X}_0)$  because the Hamiltonian is a constant of motion, and  $H_i(\mathbf{X}_0) = V_i(\mathbf{R}_0)$  because  $\mathbf{P}_0 = \mathbf{0}$ . Then,

$$S(t) = S_{\text{red}}(t) - \Delta E t, \quad (14)$$

where

$$\Delta E = V_2(\mathbf{R}_0) - V_1(\mathbf{R}_0) \quad (15)$$

is the energy gap at  $\mathbf{R}_0$  and

$$S_{\text{red}}(t) = \int_{\mathbf{R}_0}^{\mathbf{R}_2(t)} \mathbf{P}_2^T \cdot d\mathbf{R} - \int_{\mathbf{R}_0}^{\mathbf{R}_1(t)} \mathbf{P}_1^T \cdot d\mathbf{R} - \bar{\mathbf{P}}^T \cdot \Delta \mathbf{R} \quad (16)$$

$$= \oint_{\mathbf{C}} \mathbf{P}^T \cdot d\mathbf{R} \quad (17)$$

is the reduced action equal to the signed area within the closed curve  $\mathbf{C}$  consisting of the two classical paths connecting  $\mathbf{X}_0$  with  $\mathbf{X}_i(t)$  ( $i \in \{1, 2\}$ ) and a straight line connecting  $\mathbf{X}_1$  and  $\mathbf{X}_2$  (see Fig. 2 of the main text, where the indices 1, 2 are replaced with general indices  $i, j$ ) [16].

#### IV. CHARGE MIGRATION IN PROPIOLAMIDE MOLECULE

Figure 2 shows the first four ionic states of propiolamide. The next excited cationic state is located at 14.5 eV. The strong electron correlation between valence orbitals in the neutral propiolamide leads to appearance of the almost equal in weights one-hole configurations in the ionic states. Therefore, as for the propiolic acid, an ultrashort (sudden) ionization of the molecule will inevitably create an electronic wave packet and trigger dynamics of the electron density between the carbon triple bond and amide moiety of the system.

One way to describe and visualize the dynamics of electrons along the molecular chain is to compute the hole density of the system. The latter is defined as the difference between the electronic density of the system before ionization (the neutral) and the electronic density of the cation [17–19]

$$Q(\mathbf{r}, t) = \int_{\mathbf{R}} d\mathbf{R} (\langle \Psi^N(\mathbf{R}) | \hat{\rho}(\mathbf{r}, \mathbf{R}) | \Psi^N(\mathbf{R}) \rangle - \langle \Psi^{N-1}(\mathbf{R}, t) | \hat{\rho}(\mathbf{r}, \mathbf{R}) | \Psi^{N-1}(\mathbf{R}, t) \rangle), \quad (18)$$

where  $\hat{\rho}(\mathbf{r}, \mathbf{R})$  is the one-body electronic density operator,  $\Psi^N(\mathbf{r}, \mathbf{R})$  is the stationary ground molecular state of the neutral, and  $\Psi^{N-1}(\mathbf{R}, t)$  is the time-dependent molecular wavefunction of the ion. Assuming that both electronic states and the density operator  $\hat{\rho}(\mathbf{r}, \mathbf{R})$  have a weak dependence on nuclear coordinates  $\mathbf{R}$ , Eq. (18) can be further simplified as

$$Q(\mathbf{r}, t) \approx \langle \Phi_0^N | \hat{\rho}(\mathbf{r}) | \Phi_0^N \rangle - \sum_{i,j} \chi_{ij}(t) \langle \Phi_i^{N-1} | \hat{\rho}(\mathbf{r}) | \Phi_j^{N-1} \rangle, \quad (19)$$

where  $\Phi_0^N$  is the ground electronic state of the neutral,  $\Phi_i^{N-1}$  are the electronic states of the ion, and coefficients  $\chi_{ij}(t)$  denote the populations of electronic states when  $i = j$  and the electronic coherences when  $i \neq j$ .

The hole density computed for ionization out of HOMO and HOMO–1 of propiolamide is shown in Fig. 3. In the top panel of the Fig. 3 we plot evolution of positive charge, Eq. (18), taking into account *all* electronic states of the propiolamide in the fixed geometry framework. Middle panel illustrates fixed geometry calculations performed by truncating full ionic subspace to the two lower electronic states in both symmetries. A good agreement between top and middle panels of Fig. 3 verifies the validity of considered electronic dynamics in the truncated basis. Bottom panel shows electronic dynamics in truncated basis with moving nuclei calculated by Eq. (19) using electronic coherences evaluated by the TGA scheme described in the main text. We see that in both symmetries the nuclear motion leads to fast decoherence of electronic oscillations.

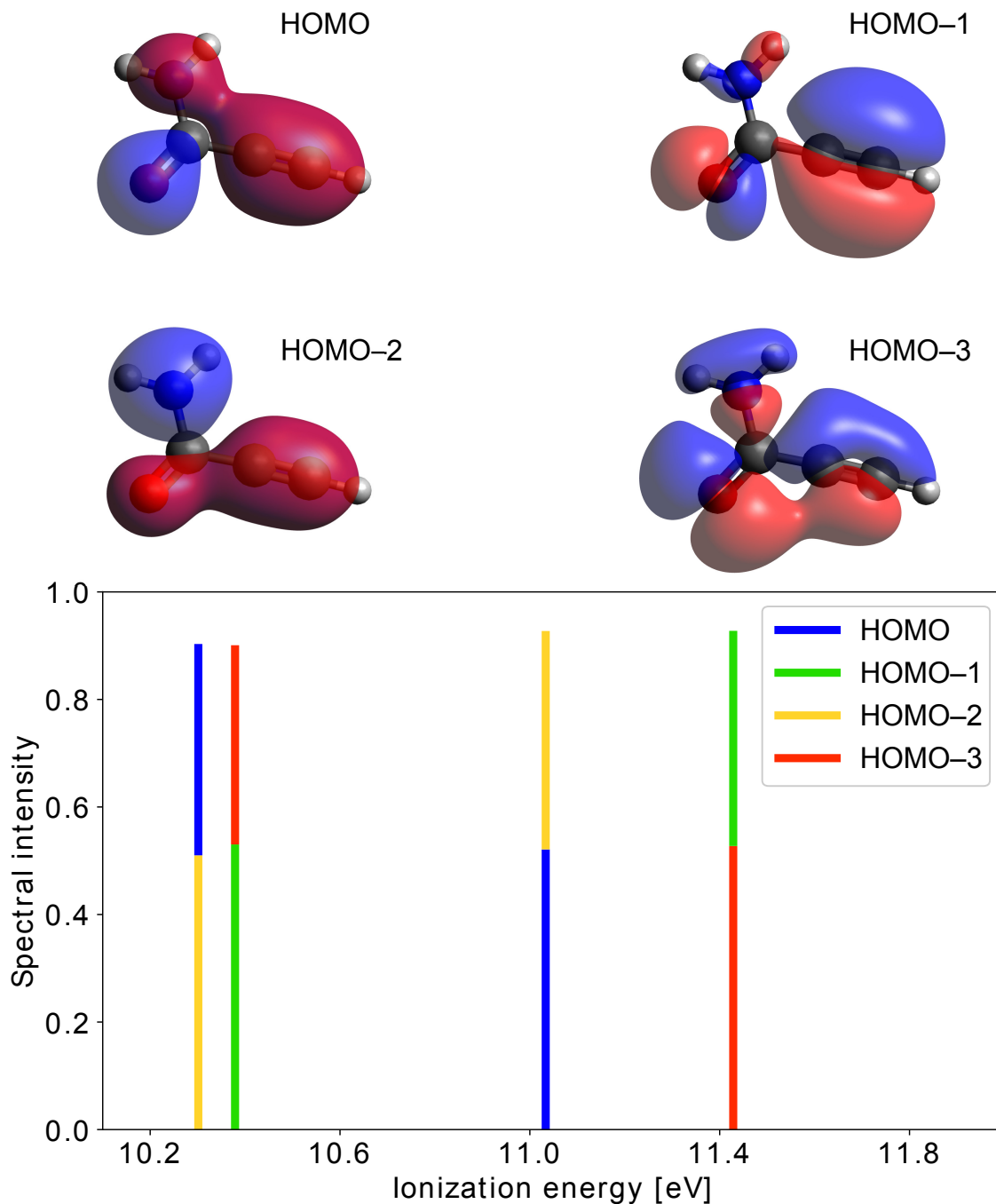
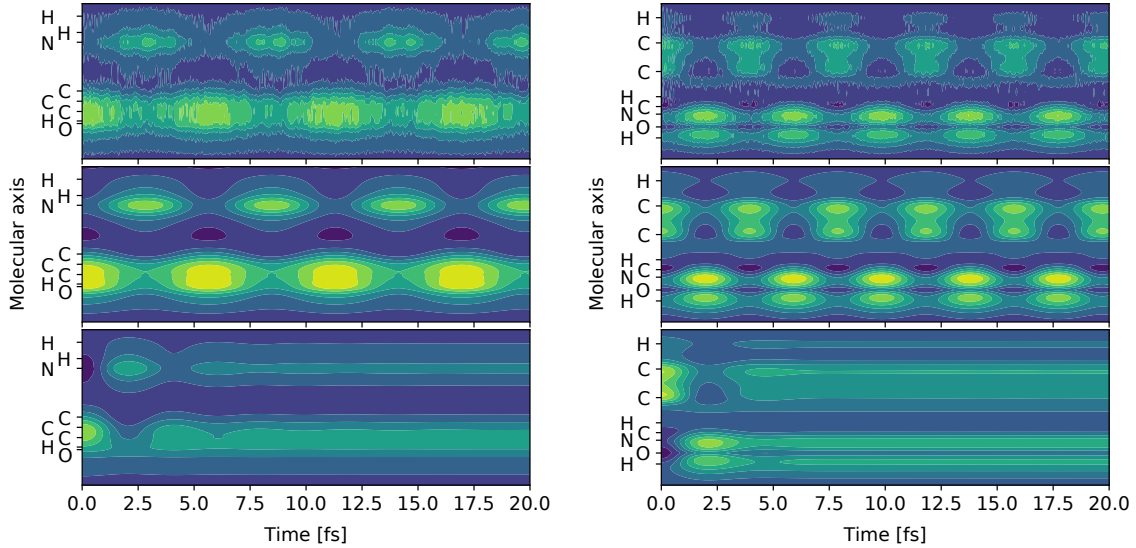
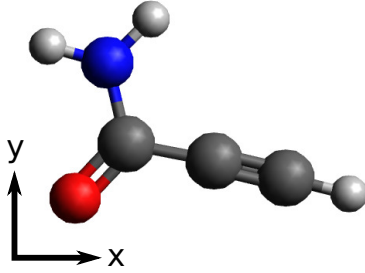


FIG. 2: First four cationic states of the propiolamide computed using the *ab initio* many-body Green's function ADC(3) method. The second and fourth states belong to the  $A'$  symmetry, while the first and third states to  $A''$ . The next ionic state is located at 14.5 eV. The spectral intensity is defined as the combined weight of all one-hole configurations in the configuration-interaction expansion of the ionic state. The orbitals involved in the hole-mixing are also depicted.



(a) Ionization out of HOMO,  $y$  direction.

(b) Ionization out of HOMO-1,  $x$  direction.

FIG. 3: Time evolution of the hole density, Eq. (19), along different directions of propiolamide molecule, after an ionization out of (a) HOMO and (b) HOMO-1. Different panels show results of electronic dynamics calculations obtained under different assumptions. Top panels: Full electronic basis with fixed nuclei. Middle panels: Truncated electronic basis with fixed nuclei. Bottom panels: Truncated electronic basis with moving nuclei.

## V. COMPARISON OF TGA WITH VMCG

The performance of the vMCG method in the VC model of propiolic acid was compared with the MCTDH benchmark and the TGA results. Both single-set ansatz (where only one set of Gaussian functions is used for all electronic states) and multi-set ansatz (where the Gaussians on different states evolve separately) were considered. The single-Hessian TGA approach used in the present study can be considered as a special case of the vMCG method. In particular, a *single* Gaussian function with *relaxed* parameters is used for each involved

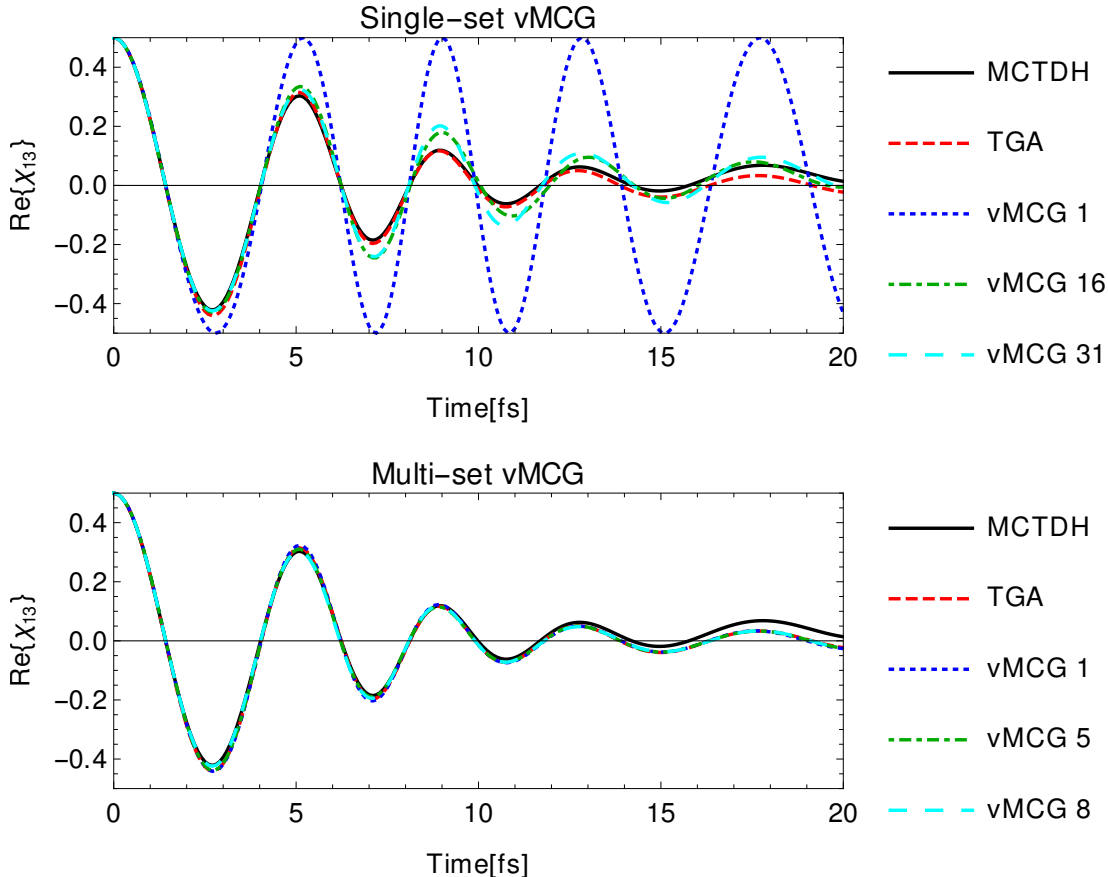


FIG. 4: Electronic coherence in the full-dimensional vibronic coupling model of the propiolic acid. Comparison between the MCTDH benchmark, the TGA result, and vMCG calculations with variable number of frozen Gaussian basis functions. Top panel: Single-set vMCG calculations with 1, 16, and 31 Gaussians. Bottom panel: Multi-set vMCG calculations with 1, 5, and 8 Gaussians per state.

electronic state (multi-set ansatz), the center of each Gaussian follows *classical* (i.e., non-variational) molecular dynamics trajectory, all nonadiabatic couplings between surfaces are neglected, and the potential is assumed to be locally harmonic with a constant (reference) Hessian. Indeed, due to the generality of vMCG, nearly all Gaussian-based methods can be considered extensions or special cases of it.

vMCG calculations were performed in Quantics v1.2 package [20, 21]. Default options in Quantics were used for the initial positions and widths of the Gaussian basis functions: shells in position space with the central Gaussian fitting exactly the initial state (widths of all Gaussians were equal to the width of the initial state).



Figure 4 shows that the single-set vMCG approach used previously in Ref. [9] (Gaussian functions with frozen parameters, the center of each Gaussian follows non-classical variational equations of motion) cannot reproduce the exact benchmark results even with a rather large number of basis functions, whereas the multi-set methods perform better already with a single Gaussian function per state. Interestingly, using more Gaussians in the multi-set vMCG method converges only very slowly to the exact MCTDH non-adiabatic result. Multi-set calculations with more than 8 Gaussians per state were failing—further convergence of the vMCG results would require careful tuning of the initial parameters of the Gaussian functions (see, e.g., Ref. [10]). Remarkably, the TGA, which uses only a single classical trajectory (for each of the two states), yields in this system better results than the single-set version of vMCG with 31 variational trajectories and as good results as the single-set version of vMCG with 8 variational trajectories. This is probably due to the flexible width of the thawed Gaussian which captures more anharmonicity than a single frozen Gaussian [22] (but which can, in multi-trajectory coupled thawed Gaussian methods, result in numerical instabilities).

As for the cost of the calculations, the single-set approach is computationally advantageous when a very large number of electronic states is considered—however, there is no guarantee that the method will converge within a feasible number of basis functions. In contrast, the multi-set methods employ a different Gaussian basis on each involved electronic state and, therefore, much fewer basis functions per state are needed. According to Fig. 4, one can expect that using only one Gaussian per surface provides a good estimate of the short-time electronic coherence. In systems with stronger anharmonic effects and larger differences between surface curvatures, an additional degree of accuracy can be achieved by using the TGA, which allows the Gaussian wavepacket to spread or contract, but requires additional Hessian evaluations (one per surface in the single-Hessian version). Finally, since the TGA neglects nonadiabatic coupling, wavepacket propagations in different electronic states are independent and can be performed in parallel and only those states that are populated initially have to be considered, which makes the calculations extremely efficient. Interestingly, the importance of nonadiabatic couplings and thus the applicability of the TGA to the system under study can be evaluated on the fly with an efficient semiclassical approach to estimate adiabaticity (the so-called multiple-surface dephasing representation [23, 24]). This method does not even require calculations of Hessians and operates only with classical

molecular dynamics trajectories.

---

- [1] E. J. Heller, *J. Chem. Phys.* **62**, 1544 (1975).
- [2] T. Begušić, J. Roulet, and J. Vaníček, *J. Chem. Phys.* **149**, 244115 (2018).
- [3] V. Despré, N. V. Golubev, and A. I. Kuleff, *Phys. Rev. Lett.* **121**, 203002 (2018).
- [4] H.-D. Meyer, U. Manthe, and L. S. Cederbaum, *Chem. Phys. Lett.* **165**, 73 (1990).
- [5] M. Beck, A. Jäckle, G. Worth, and H.-D. Meyer, *Phys. Rep.* **324**, 1 (2000).
- [6] I. Burghardt, H.-D. Meyer, and L. S. Cederbaum, *J. Chem. Phys.* **111**, 2927 (1999).
- [7] G. A. Worth and I. Burghardt, *Chem. Phys. Lett.* **368**, 502 (2003).
- [8] G. Richings, I. Polyak, K. Spinlove, G. Worth, I. Burghardt, and B. Lasorne, *Int. Rev. Phys. Chem.* **34**, 269 (2015).
- [9] M. Vacher, M. J. Bearpark, M. A. Robb, and J. a. P. Malhado, *Phys. Rev. Lett.* **118**, 083001 (2017).
- [10] A. J. Jenkins, K. E. Spinlove, M. Vacher, G. A. Worth, and M. A. Robb, *J. Chem. Phys.* **149**, 094108 (2018).
- [11] J. Schirmer, A. B. Trofimov, and G. Stelter, *J. Chem. Phys.* **109**, 4734 (1998).
- [12] A. Canal Neto, E. Muniz, R. Centoducatte, and F. Jorge, *J. Mol. Struct. THEOCHEM* **718**, 219 (2005).
- [13] P. Hohenberg and W. Kohn, *Phys. Rev.* **136**, B864 (1964).
- [14] P. J. Stephens, F. J. Devlin, C. F. Chabalowski, and M. J. Frisch, *J. Phys. Chem.* **98**, 11623 (1994).
- [15] M. J. Frisch, G. W. Trucks, H. B. Schlegel, G. E. Scuseria, M. A. Robb, J. R. Cheeseman, G. Scalmani, V. Barone, G. A. Petersson, H. Nakatsuji, X. Li, M. Caricato, A. V. Marenich, J. Bloino, B. G. Janesko, R. Gomperts, B. Mennucci, H. P. Hratchian, J. V. Ortiz, A. F. Izmaylov, J. L. Sonnenberg, D. Williams-Young, F. Ding, F. Lipparini, F. Egidi, J. Goings, B. Peng, A. Petrone, T. Henderson, D. Ranasinghe, V. G. Zakrzewski, J. Gao, N. Rega, G. Zheng, W. Liang, M. Hada, M. Ehara, K. Toyota, R. Fukuda, J. Hasegawa, M. Ishida, T. Nakajima, Y. Honda, O. Kitao, H. Nakai, T. Vreven, K. Throssell, J. A. Montgomery, Jr., J. E. Peralta, F. Ogliaro, M. J. Bearpark, J. J. Heyd, E. N. Brothers, K. N. Kudin, V. N. Staroverov, T. A. Keith, R. Kobayashi, J. Normand, K. Raghavachari, A. P. Rendell, J. C.

- Burant, S. S. Iyengar, J. Tomasi, M. Cossi, J. M. Millam, M. Klene, C. Adamo, R. Cammi, J. W. Ochterski, R. L. Martin, K. Morokuma, O. Farkas, J. B. Foresman, and D. J. Fox, “Gaussian 16 Revision C.01,” (2016), gaussian Inc. Wallingford CT.
- [16] E. Zambrano and A. M. Ozorio de Almeida, *Phys. Rev. E* **84**, 045201(R) (2011).
- [17] L. Cederbaum and J. Zobeley, *Chem. Phys. Lett.* **307**, 205 (1999).
- [18] J. Breidbach and L. S. Cederbaum, *J. Chem. Phys.* **118**, 3983 (2003).
- [19] A. I. Kuleff, J. Breidbach, and L. S. Cederbaum, *J. Chem. Phys.* **123**, 044111 (2005).
- [20] G. A. Worth, K. Giri, G. W. Richings, I. Burghardt, M. H. Beck, A. Jäckle, and H.-D. Meyer, “The QUANTICS Package, Version 1.1,” (2015).
- [21] G. Worth, *Comput. Phys. Commun.* **248**, 107040 (2020).
- [22] S. Han, D. Xie, and H. Guo, *J. Chem. Theory Comput.* **14**, 5527 (2018).
- [23] T. Zimmermann and J. Vaníček, *J. Chem. Phys.* **132**, 241101 (2010).
- [24] T. Zimmermann and J. Vaníček, *J. Chem. Phys.* **136**, 094106 (2012).